Preferred citation: H. Tomimasu, P. Luner and R.B. Hanna. Rapid imaging of mass distribution in paper by electron beams. In **Fundamentals of Papermaking**, *Trans. of the IXth Fund. Res. Symp. Cambridge, 1989*, (C.F. Baker & V. Punton, eds), pp 159–194, FRC, Manchester, 2018. DOI: 10.15376/frc.1989.1.159.

RAPID IMAGING OF MASS DISTRIBUTION IN PAPER BY ELECTRON BEAMS

Hiroshi Tomimasu*, Philip Luner and Robert B. Hanna
Empire State Paper Research Institute, State University of New York, College of Environmental Science and Forestry, Syracuse, New York 13210, U.S.A.

*Visiting Scientist, Mutsubishi Paper Mills Ltd.

ABSTRACT

A rapid method to measure the distribution of mass density of paper and paper board was developed. Paper is irradiated with electron beams with energies from 50 to 200 keV and the attenuation of the electron beams by the paper is detected by a photographic film and a real-time TV monitor system. The image of the attenuation of the electron beams (electrograph) is converted into the distribution of mass density through a basis weight calibration. By this method, the basis weight distribution of paper and paper board from 0 to 400 g/m^2 was obtained in less than 1 second with both detectors. It was found that the electrograph gives very similar information as beta-radiograph. Experiments to optimize the imaging of the distribution of mass density of paper by electron beams are described along with the relevant physics.

INTRODUCTION

Many attempts have been made to measure the uniformity of fiber distribution objectively using light transmission. The reader is referenced to the paper by Corte (1) for a good review on the subject. However, light transmission in paper is affected by many factors such as the degree of bonding, pressing and the presence of scattering fillers (2, 3, 4). Other methods for assessing mass variations rather than opacity variations should therefore be used to describe the fiber distribution within the sheet. In the early 1960's Corte and

Herdman (5, 6) introduced the distribution of mass density in contrast to the distribution of optical density. This was obtained by measuring the attenuation of beta-radiation through paper, either directly or by using photographic film (7, 8, 9). This method has been used by many investigators such as Tydeman (10), Norman and Wahren (2), Yang and Thorpe (11), Sara (3), Herdman and Corte (5), Murata and Nakata (12), Bergh (13), and Gorres (14) with success. However, this method may take 4 to 24 hours and the distribution of mass density of thick paper samples the basis weight of which is above 150 g/m^2 cannot be obtained by this method. In the mill, beta-gages are used for measuring the distribution of mass density in the paper. The system usually measures areas as large as 25 cm^2 and gives the average and the variation of the basis weight, but it does not give the variation in small areas within the sample.

In the field of electron microscopy, a technique to measure the thickness or the density of a very thin sample by TEM (Transmission Electron Microscope) was developed by Marton and Schiff (15). This technique has been studied closely and applied to determine the thickness, the density, and the dry mass of biological samples and synthesized latices by Zeitler and Bahr (16, 17, 18, 19), Bahr *et al* (20), Edie and Karlsson (21, 22), and Linders *et al* (23, 24). However, according to Zeitler and Bahr (17), this technique has a limitation in sample thickness. Only the sample which is less than 0.4 microns in thickness can be measured by this method. As paper samples are far thicker than the materials used, this method could not be used to measure the distribution of mass density of paper.

This paper presents a new method of imaging paper by electron beams. The following criteria have guided the development of the systems. The distribution of mass density of paper should be determined by fast or real-time measurement. The method should cover a wide range of basis weight with a high image resolution. The method should be safe and easy to operate. The system should have the ability to supply digitized data for further processing and to distinguish between the different components in paper.

THEORY

Difference between beta-rays and electron beams

Beta-rays are emitted by radioactive nuclei such as ^{3}H, ^{14}C, ^{85}Kr, ^{147}Pm, and ^{204}Tl. The beta-spectrum is continuous because the transition energy is shared between an electron and a neutrino. Thus, each of these may carry away any part of the available energy from 0 to E_{max}. For example, the energy spectrum of ^{14}C beta-rays is shown in Fig.1 (25). The maximum energy is 155 keV for ^{14}C beta-rays. On the other hand, electron beams generated by electron guns are nearly monoenergetic. In the normal electron gun operation condition, an energy distribution of 1 to 2 eV is observed (26). However, it is trivial compared to that of beta-rays. The energy distribution of a 80 keV electron beam is also shown in Fig. 1. The difference in energy distribution greatly affects the basis weight calibration which is discussed in the following sections.

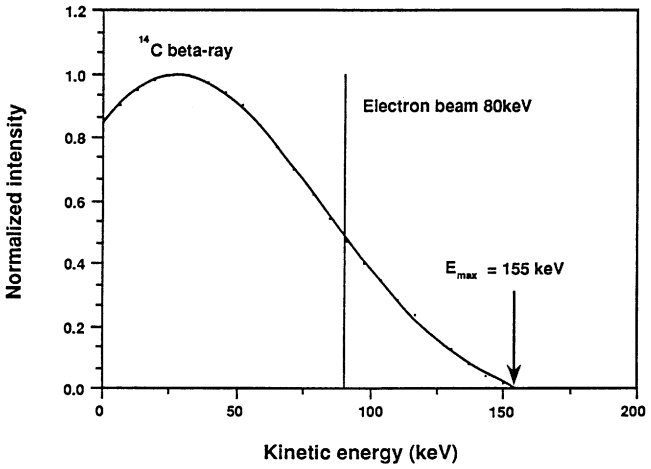

Fig.1 Energy spectra of ^{14}C beta-ray and electron beam of 80 keV.

The flux intensity of electron beams are much higher than that of beta-rays. The highest nominal activity of ^{14}C plastic beta-source which is commercially available is at most 100 $\mu Ci/cm^2$. A ^{14}C plastic beta-source with a nominal activity of 100 $\mu Ci/cm^2$ gives approximately 3.33×10^4 electron/cm^2 second. On the other hand, an ordinary transmission electron microscope at a current density of 60 pA/cm^2 gives 3.75×10^8 electron/cm^2 second. This indicates that the exposure time can be drastically reduced by using an electron gun instead of a beta-source.

Attenuation of electron energy

The energy range of electrons can be conveniently divided into these three regions (27):

1. nonrelativistic : $E < 100$ keV
2. relativistic : 100 keV $< E <$ 2 MeV
3. ultra-relativistic : $E >$ 2 MeV.

Since we are interested in the energy range from 50 keV to 200 keV, both the nonrelativistic and the relativistic region should be considered. However, the relativistic effects are so significant in this energy range that the relativistic formulations were used here.

The kinetic energy of an electron E is given by

$$E = eU \tag{1}$$

where e is the charge of electron (1.6022×10^{-19} C) and U is the accelerating voltage (V). For example, electrons accelerated at 100 kV of accelerating voltage have 100 keV of kinetic energy.

An electron passing through matter loses energy partly by collision and partly by radiation. The ratio of energy loss by the two processes is given by (28):

$$\frac{\left(-\frac{dE}{dx}\right)_{\text{radiation}}}{\left(-\frac{dE}{dx}\right)_{\text{collision}}} = \frac{E\,Z}{800} \tag{2}$$

where Z is the atomic number of the element and E is in MeV. The ratio of energy loss by radiation and by collision for electron beams of 100 keV in cellulose is 1/1954 and hence the energy loss by radiation is negligible. Therefore, only the energy loss by collision is dealt with here.

The mean energy loss by collision can be calculated according to the Bethe's stopping power theory (28), using the formulation of Rohrlich and Carlson (29) which was used by Berger and Seltzer (30) to prepare tables of energy losses in various materials:

$$-\frac{1}{\rho}\left(\frac{dE}{dx}\right) = \chi \frac{Z}{A}\{B + F(\gamma) - \delta\} \qquad (3)$$

where

$$\chi = \frac{2\pi N_a r_0^2 E_0}{\beta^2}$$

$$B = \ln\left(\frac{\gamma^2(\gamma+2)}{2(I/E_0)^2}\right)$$

$$F(\gamma) = 1-\beta^2 + \frac{\gamma^2/8 - (2\gamma+1)\ln 2}{(\gamma+1)^2}$$

The various symbols have the following meaning:

x = depth
ρ = density
A = atomic weight
δ = density effect correction
N_a = Avogadro's number = 6.0220×10^{23} electron/mole
E_0 = electron rest energy = 0.5110 MeV
β = velocity ratio of electron and light = $\sqrt{1 - \frac{1}{(1 + E/E_0)^2}}$
$r_0^2 = (e^2/E_0)^2 = 7.9403 \times 10^{-26}$ cm^2
$\gamma = E/E_0$
I = mean ionization energy.

Since the density effect is very small in the low energy range especially E < 200 keV (30), it was neglected here.

Paper and Mylar film which are of interest here consists of hydrogen, carbon, and oxygen, and hence Z/A for these materials is calculated as follows:

$$\frac{Z}{A} = \frac{1}{\rho} \sum_{j} \left(\frac{Zj}{Aj} \rho j \right) \tag{4}$$

where

$$\sum_{j} \rho j = \rho,$$

and Aj, Zj, and ρj are the atomic weight, the atomic number, and the density of each constituent element respectively.

The values of the mean ionization energy used here were obtained by Berger and Seltzer (30) based on the analysis of proton stopping data and are shown in Table 1.

Element	I (eV)
H	18.7
C	78.0
O	89.0

Table 1 Table of mean ionization energy.

According to Bragg's rule (31), the mean energy loss of compounds is assumed to be the sum of the losses in the constituent elements and is given by

$$\ln I = \frac{\sum_j \left(\frac{Z_j}{A_j} \rho_j \ln I_j\right)}{\sum_j \left(\frac{Z_j}{A_j} \rho_j\right)} \qquad (5)$$

where Ij is the mean ionization energy of each constituent element. The values of Z/A, ρ, and I for paper and Mylar film which is used as a reference material for a basis weight calibration are listed in Table 2.

Parameters	Cellulose $(C_6H_{10}O_5)_n$	Mylar film $(C_{10}H_8O_4)_n$
Z/A	0.531 mole/g	0.521 mole/g
ρ	1.56 g/cm^3	1.43 g/cm^3
I	70.25 eV	72.58 eV

Table 2 Parameters used for calculating the energy attenuation of electrons.

According to the CSDA (Continuous Slowing-Down Approximation) method (28), the penetration depth of the electron R_B can be obtained by graphical integration according to the equation:

$$R_B = \int_0^E \frac{1}{-\frac{1}{\rho}\left(\frac{dE}{dx}\right)} dE \qquad (6)$$

The relationship between the kinetic energy of electrons and the range of penetration for cellulose and Mylar film is shown in Fig. 2.

The curve showing the energy attenuation of electrons in cellulose and Mylar film was obtained by plotting the remaining electron energy against the penetration depth (basis weight) during the integration process mentioned above. Fig. 3 shows the energy attenuation at various electron energy for cellulose. Mylar film gave nearly similar values.

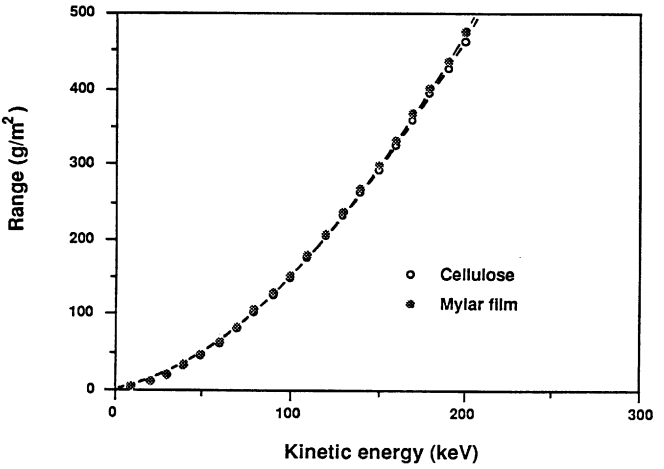

Fig.2 Range of electron beams in cellulose and Mylar film.

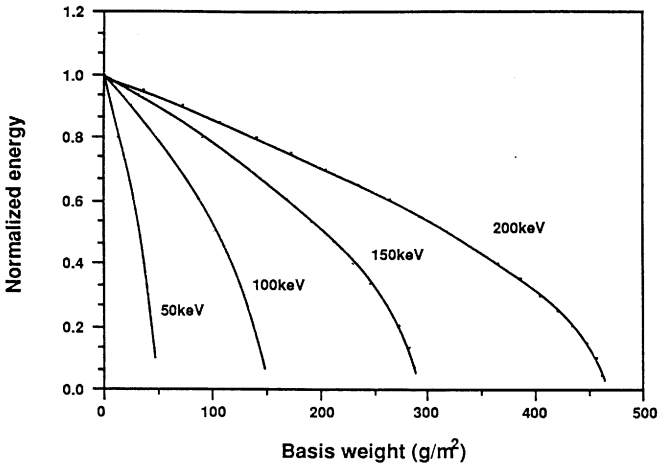

Fig.3 Attenuation of electron beams in cellulose.

Attenuation of beta-rays

In the case of beta-rays, the attenuation of its intensity is given by the exponential law:

$$I_a = I_i \, e^{-\mu w} \qquad (7)$$

where I_i and I_a are the initial intensity and the attenuated intensity of beta-rays respectively, μ is the mass absorption coefficient of the sample, and w is the basis weight of the sample. The results of calculations for cellulose and Mylar film are shown in Fig. 4. As indicated by the comparison of Fig. 3 and 4, the attenuation of electron beams is very different from that of beta-rays, and indicates that the attenuation of electron beams would give better basis weight resolution than beta-rays.

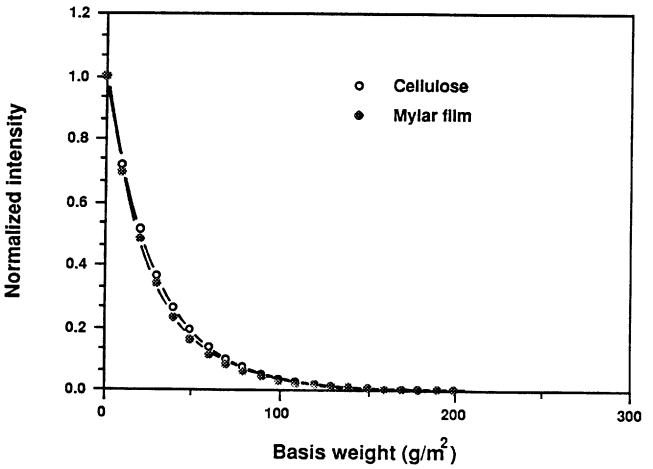

Fig. 4 Attenuation of beta-rays in cellulose and Mylar film.

EXPERIMENTAL

Several TEM systems were used to generate electron beams to obtain a wide energy range with uniform intensity distribution over a wide area. The TEM system used here and operation conditions for each system are as follows:

RCA EMU-4
- Accelerating voltage : 50 and 100 kV
- Photometer : 2.0
- Magnification : X 10,000
- Exposure time : 1.0 to 5.0 seconds

JEOL JEM-2000EX
- Accelerating voltage : 80, 100, 150, and 200 kV
- Current density : 30 pA/cm^2
- Magnification : X 10,000
- Exposure time : 0.5 to 2.0 seconds

PHILIPS EM400
- Accelerating voltage : 60, 80, 100, and 120 kV
- Current density : 50 pA/cm^2
- Magnification : X 8,000
- Exposure time : real-time imaging with a TV monitor system.

Photographic films and a TV monitor system were used as electron beam detectors to image the distribution of mass density.

Photographic film system (Electrography)

The configuration of the photographic film system is shown in Fig. 5. Two films having different characteristics, Kodak Industrex-R (Kodak IR) film and Mitsubishi Electron Microscope (Mitsubishi EM) film were used to obtain an electron transmission image of the sample namely electrograph (24).

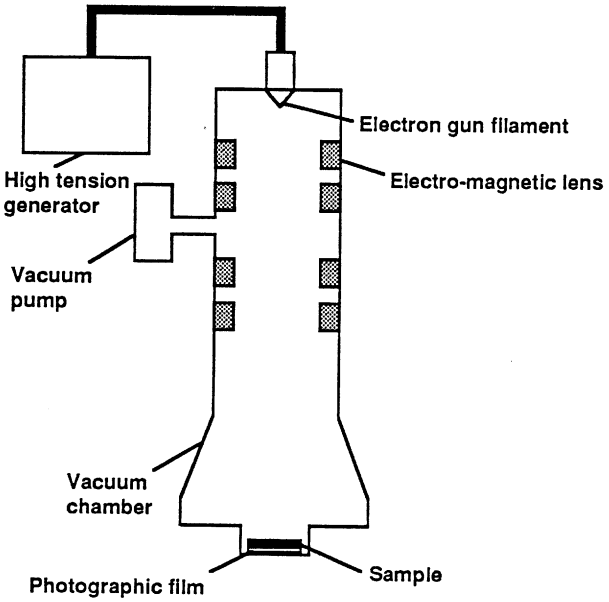

Fig.5 Configuration of the electrography system.

A sample (6 cm X 6 cm) was attached to the emulsion layer of a photographic film with adhesive tapes to obtain a good contact between the sample and the film. A template which is attached with a Mylar film wedge with different basis weights which is a reference for a basis weight calibration was placed on the photographic film. The photographic film was then loaded in a film container, inserted into a TEM exposure chamber, and irradiated by electron beams. After the exposure, the photographic film was developed in a standard way. The image on the film was digitized by an Optronics Photomation System P-1700 drum scanner to give 256 gray levels. The digitized data were transfered to a Sun 3/110 work station and processed to evaluate the uniformity of the distribution of mass density with the algorithm presented by Cresson (32).

TV monitor system

The configuration of the TV monitor system is shown in Fig. 6. A Gatan Model 673 TV Monitor System was used as an electron beam detector to obtain an electron transmission image of the sample.

A sample was placed on the aluminium coated YAG (Yttrium Aluminium Garnet) fluorescent screen (which efficiently converts electron beams into visible light) and irradiated by electron beams. An electron transmission image of the sample is transformed into a light image by the YAG screen and transfered to a CCD image sensor in a CCTV camera system through an optical fiber coupling system. The detected image by the CCTV system is transfered to a Coreco Oculus 200 image processing board which is hosted by an IBM PC computer, and digitized to give 256 gray levels for further processing.

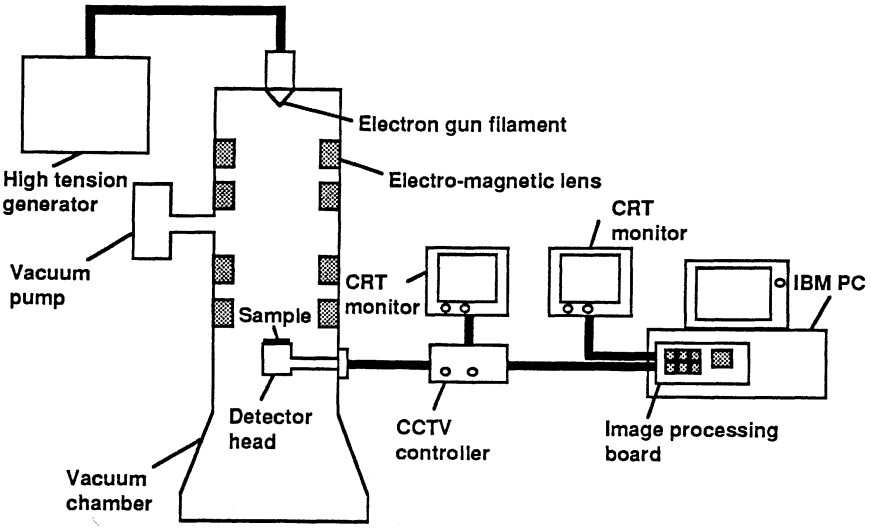

Fig.6 Configuration of the TV monitor system.

Beta-radiography

A ^{14}C labeled poly-MMA beta-source (102 mm X 102 mm X 1mm, nominal activity of 6.17 mCi, made by Amersham Co.) was used to obtain beta-radiographs. A sample was overlayed by the template attached with a Mylar film wedge and sandwiched between the beta-source and a photographic film. The sandwich was then placed in the aluminium exposure chamber for several hours. After the exposure, the photographic film was developed in a standard way. The image on the film was digitized by the drum scanner to give 256 gray levels, and the digitized data was transfered to the work station and processed as mentioned above.

RESULTS AND DISCUSSION

Since the energy attenuation of electrons in the Mylar film is very similar to that in cellulose, only a Mylar film was used to study the basic characteristics of the energy attenuation of electron beams.

Photographic film system (Electrography)

Exposure time

Theoretical calculations showed that exposure time can be drastically reduced by using electron beams instead of ^{14}C beta-rays. Therefore, the exposure time required to obtain an electrograph in a TEM was compared to that required to obtain a beta-radiograph. The results in Fig. 7 show that 1.4 seconds is required to obtain an optical density of 2.0 for electron beams, while 5 hours is required for a beta-radiograph with the same film. The ratio of exposure time is about 1:13000, which agrees with the theoretical calculation. Since the current density of the electrons in the TEM can be increased, the exposure time can be reduced further. This gives the potential for real-time imaging of the distribution of mass density of paper.

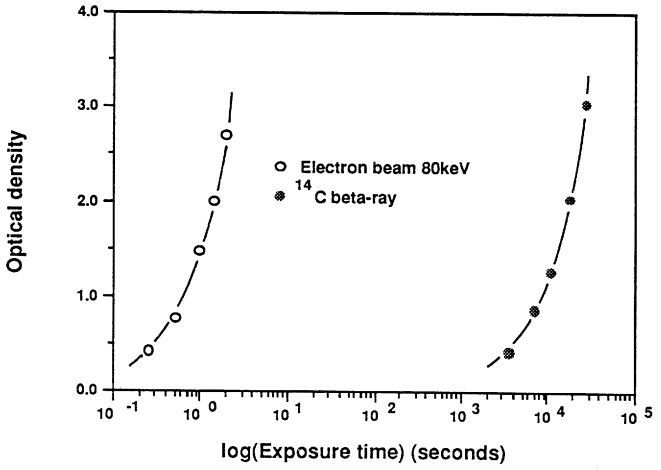

Fig.7 Comparison of exposure time between electron beams (80 keV, 30 pA/cm^2) and ^{14}C beta-rays (6.17 mCi).

Uniformity of electron beam intensity over the imaging area

A TEM can give a very uniform electron beam over a wide imaging area. The uniformity of the electron beam intensity at each point in the imaging area was measured by a blank exposure to a photographic film. The optical densities of each point in the film was measured by microdensitometry. If focusing is proper and the magnification is high enough, the variation of the electron beam intensity over the whole imaging area was found to be less than 5 %. This is in the same range of variation as for the ^{14}C plastic beta-source. The electron beam intensity in the time scale was also found to be very stable and its fluctuation was less than 1 % under standard operating conditions, which indicates that this method can give reproducible data.

Effect of electron energy

In order to study the effect of electron energy on the characteristics of the electrograph, the accelerating voltage was changed from 50 to 200 kV. Electrographs at various energy of electrons for a Mylar film wedge were obtained with Kodak IR film. The optical density of corresponding basis weight was measured by microdensitometry, normalized by adjusting the initial intensity (basis weight = 0 g/m^2) to 1.0, and plotted against the basis weight in Fig. 8. Unexpectedly, the experimental energy attenuation curves in the Mylar film showed peaks and tails, which were not observed in the theoretical attenuation curves shown in Fig. 3. The tail originates from the fluctuation of collision probability for each electron. This was proved by the Monte Carlo simulation of electron penetration in matter (33).

Photographic films are comprised of a photo-sensitive emulsion layer containing silver halides and organic binders, and base film such as poly-ester. The emulsion layer is very thin (around 10 microns) and the average atomic number of the layer is relatively low. It therefore absorbs only a part of the energy of the electrons. The energy of electrons which is absorbed in a very thin layer can be obtained by the differentiation of the energy attenuation curve of electrons for a given penetration depth and is shown in Fig. 9. A comparison of Fig. 8 and 9 indicates that the peak originates from a detector response, in another word a structure of the photographic film.

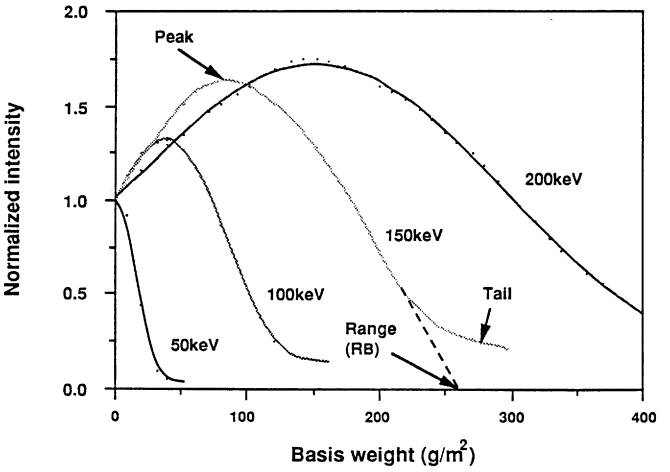

Fig.8 Energy attenuation curve for various electron energies with Kodak IR film.

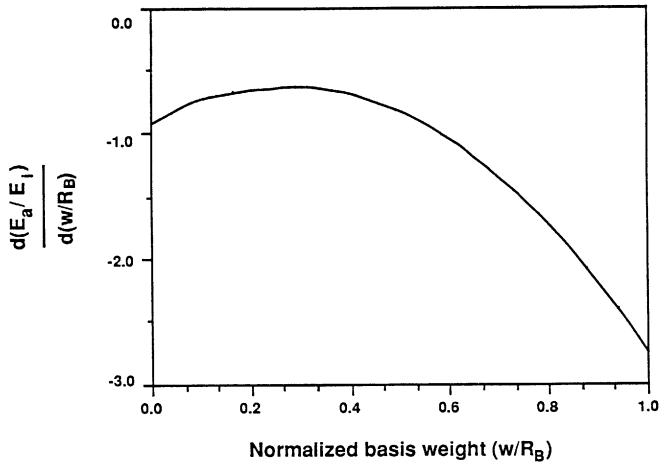

Fig.9 Differentiated energy attenuation curve of electrons.

Fig. 8 also indicates that the measurable basis weight range can be varied by changing the electron energy. This is one of the advantages of electron beams over beta-rays. In the case of beta-rays, the measurable basis weight range is more or less fixed since the energy distribution is inherently fixed. As the energy attenuation curves show peaks and tails, the measurable basis weight range is limited between the peak and the range. Fig. 10 shows the positions of the peak and the range for various electron energies. A suitable accelerating voltage for each sample is determined by using this plot.

By calculating the slope in the energy attenuation curve for various energy of electrons, the basis weight resolution was also obtained. The results in Fig. 11 indicate that the basis weight resolution is reduced as the electron energy increases. This implies that contrast of electrograph is high for low electron energies and low for high electron energies. In the case of beta-rays, the basis weight resolution is not constant over a wide basis weight range since the intensity attenuation of beta-rays follows the exponential law (Fig. 4). This may cause some errors in the basis weight calibration especially in the high basis weight range.

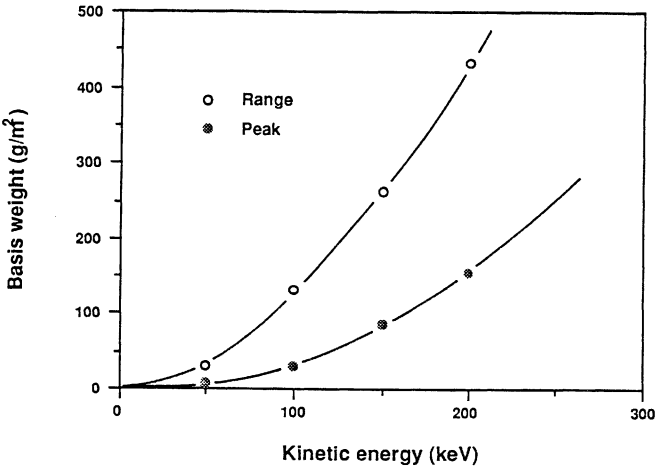

Fig.10 Range and peak for various electron energies.

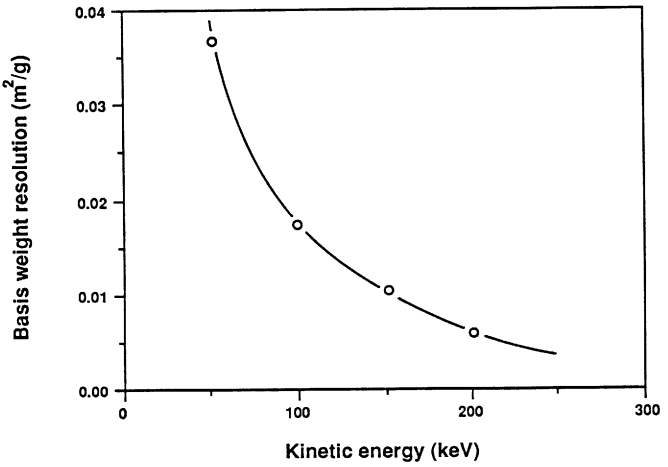

Fig.11 Basis weight resolution for various electron energies.

Multiple energy exposure

As mentioned above, beta-rays have a broad energy distribution, while electron beams are monoenergetic. This makes the difference in the shape of their energy attenuation curves. Therefore, multiple energy exposures were performed to model the beta-radiography system with electron beams. After exposing a photographic film with a Mylar film wedge to a 50 keV electron beam, the same film was exposed to a 100 keV electron beam. The exposure time at each energy level was changed and optical densities corresponding to basis weight were measured by microdensitometry. The results in Fig. 12 show that any shape of basis weight calibration curve can be obtained by combining different energies of electron beams and exposure time.

Fig. 13 shows an example of multiple energy exposure, and the addition of optical densitiies for each energy exposure was found to be the optical density of multiple energy exposure. These results show that by using multiple exposures to electron beams of different energies the measurable basis weight range can be extended.

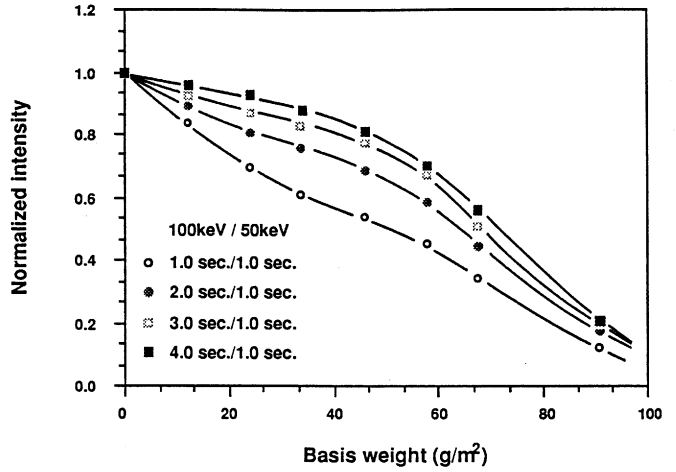

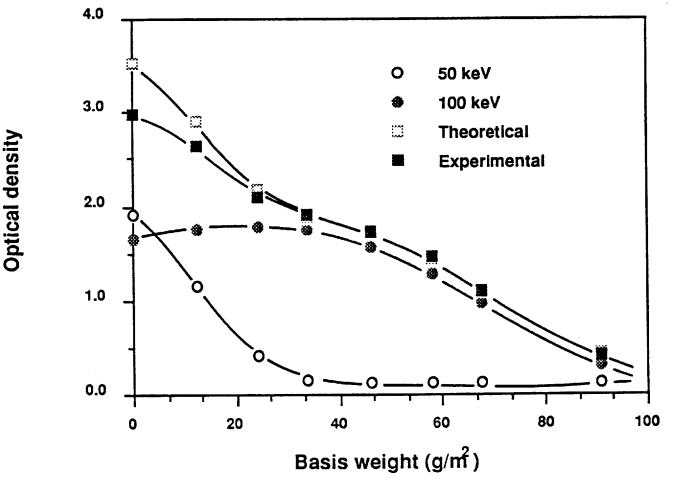

Fig.12 Basis weight calibration curves for multiple energy exposure.

Effect of photographic film

Every photographic film has a different emulsion formulation, thickness of emulsion layer, and base substrate material. These parameters define the structure and characteristics of the photographic film. Therefore, two photographic films having different structure and photographic characteristics, Kodak IR film and Mitsubishi EM film, were used to assess the effect of photographic film on the basis weight measurement by electron beams. Fig. 14 shows characteristic curves of each film at various electron energies from 80 kV to 200 kV. The Kodak IR film shows the linear characteristic curve, while the Mitsubishi EM film does not. However, the Mitsubishi EM film is more sensitive to electrons than the Kodak IR film, and hence the exposure time for the Mitsubishi EM film is shorter than the Kodak IR film.

The current density was fixed to 30 pA/cm^2 in the TEM at each electron energy. Therefore, the differences in optical densities for each level of electron energy at the same exposure time indicates the difference in sensitivity at each level. Fig. 14 indicates that both films have higher sensitivity to low energy electrons. This result is reasonable because the low energy electrons are stopped and absorb most of their energy in the the thin emulsion layer, while the high energy electrons penetrate the emulsion layer losing only a part of their energy.

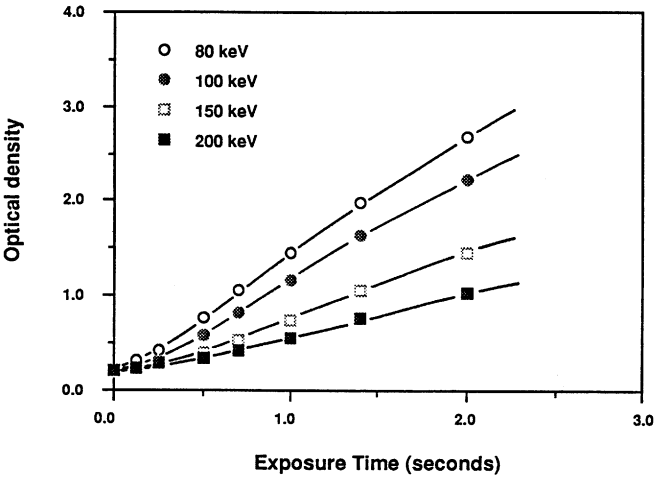

Fig.13 Basis weight calibration curve for multiple energy exposure (100 keV / 50 keV = 1.5 sec. /1.5 sec.).

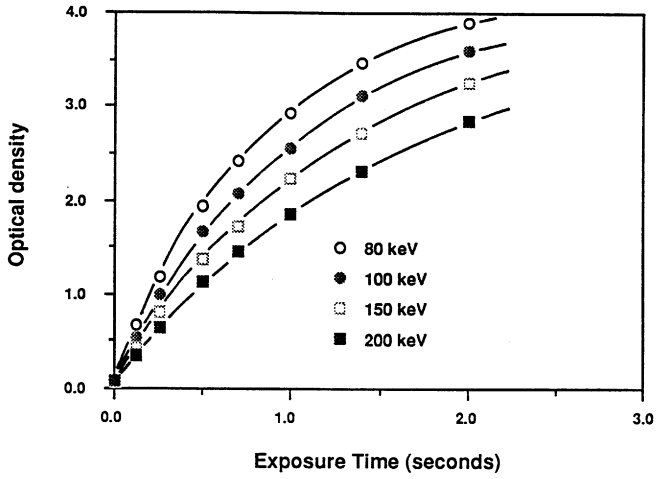

Fig.14 Characteristic curves of Kodak IR film (upper) and Mitsubishi EM film (lower) for various electron energies.

The energy attenuation curves were obtained for these two photographic films with a Mylar film wedge, and are shown in Fig. 8 and 15 respectively. Differences in curve shape are observed between the two photographic films, but no difference was observed in the position of the peak and the range. This may be explained by the difference in structure and characteristics of the emulsion formulation, thickness of the emulsion layer, and base material. However, since details about these photographic films were not available, this could not be confirmed.

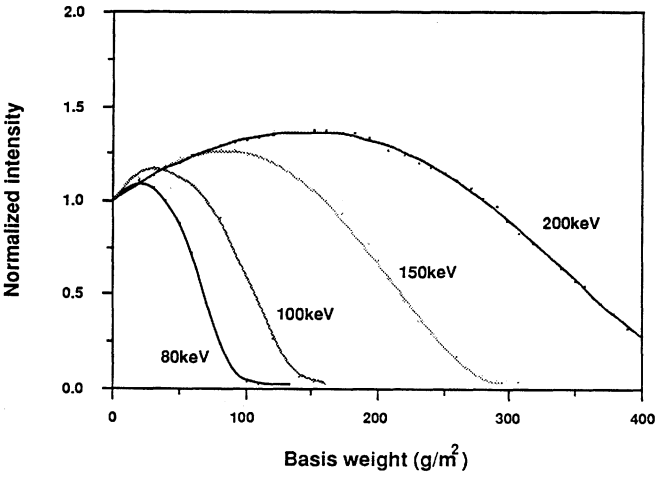

Fig.15 Energy attenuation curve for various electron energies with Mitsubishi EM film.

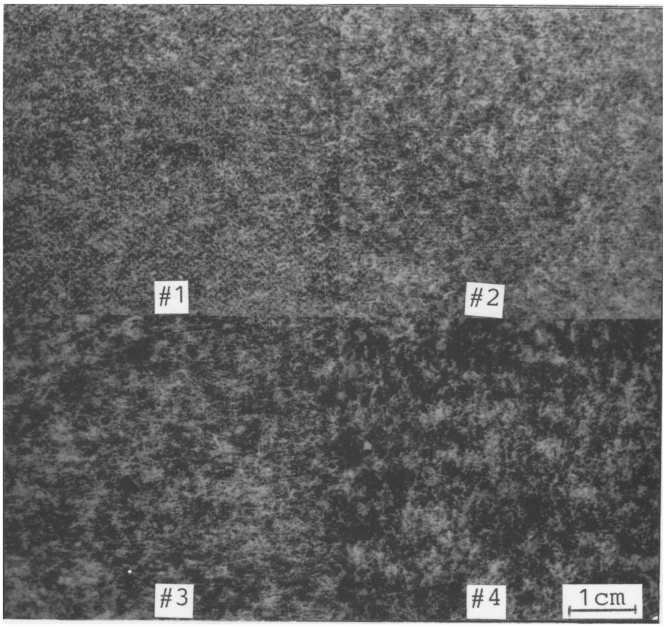

Fig.16 Electrographs of the newsprint samples.

Comparison of electrograph and beta-radiograph

Electrographs of 4 newsprint samples were compared with ^{14}C beta-radiographs in identical areas. The physical data of the samples are shown in Table 3. They were made by different formers, and hence have different formations and printability.

The accelerating voltage of electron beam was 80 kV and an exposure time of 1.0 second was required to obtain the electrographs. On the other hand, 4 hours of exposure time was required for the ^{14}C beta-radiographs. The electrographs of the samples are shown in Fig. 16.

Sample	Former	Basis weight (g/m^2)	NUI formation	Printability
#1	Twin wire	46.9	9.9	1
#2	On-top wire	46.5	9.2	2
#3	Fourdrinier	50.6	10.8	3
#4	Fourdrinier	49.8	10.5	4

Table 3 Physical data of newsprint samples. Printability is ranked from 1 (good) to 4 (poor).

The electrographs and ^{14}C beta-radiographs were digitized by a drum scanner with 0.1 mm spatial resolution to give the image size of 512 pixels X 512 pixels (51.2 mm X 51.2 mm in real size), and then the spatial resolution of the digitized image was gradually reduced to 0.2, 0.4, and 0.8 mm by averaging adjacent pixels. In order to compare the identical area, 4 pin holes of 0.1 mm diameter were made in each corner of the sample, and the electrograph and the ^{14}C beta-radiograph of the samples were carefully aligned manually according to the pin holes. No difference in physical sample dimension was observed between the two images. To find the exact overlapping point one image was moved over another by one pixel and the correlation coefficient was obtained. The point which gave the highest correlation coefficient indicated the exact overlapping point.

Now that the exact coincidence between the electrograph and the beta-radiograph is established, a comparison between the two image can be made using a variety of techniques. The correlation coefficients between electrographs and ^{14}C beta-radiographs for each sample at various spatial resolution are shown in Table 4.

Resolution	Sample			
	#1	#2	#3	#4
0.1 mm	0.787	0.644	0.671	0.751
0.2 mm	0.838	0.774	0.791	0.846
0.4 mm	0.885	0.874	0.861	0.909
0.8 mm	0.905	0.902	0.913	0.928

Table 4 Correlation coefficient between electrograph and beta-radiograph for sample #1.

A comparison of the basis weight at each point was also made for the electrograph and the ^{14}C beta-radiograph for sample #1 at various spatial resolution. Probability contour maps are shown in Fig. 17.

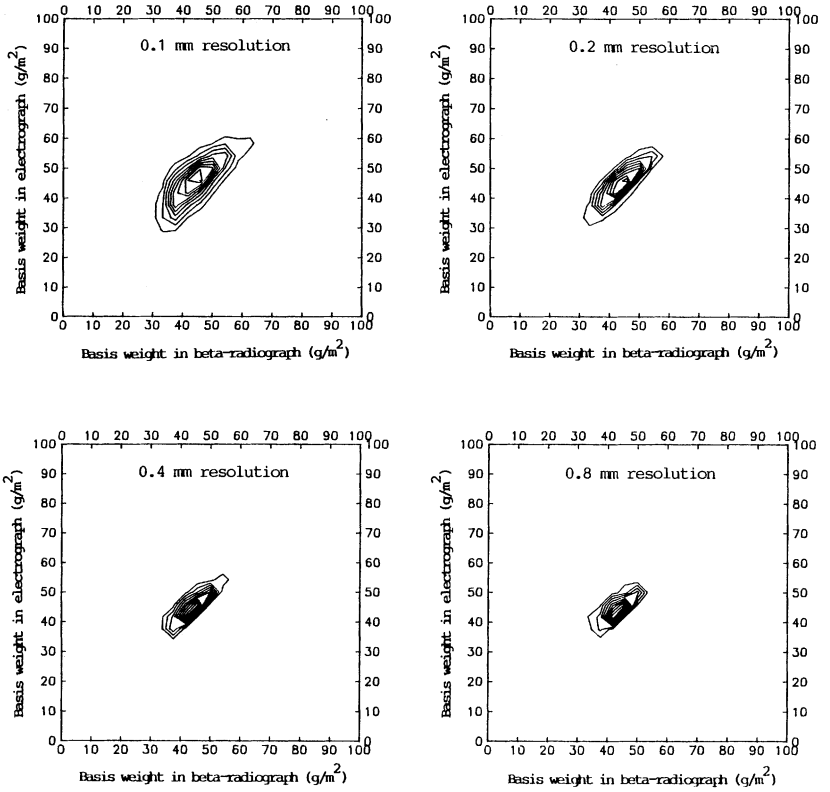

Fig.17 Comparison of electrograph and beta-radiograph at each point for sample #1.

Table 4 and Fig. 17 indicate that electrographs and ^{14}C beta-radiographs are very similar at a spatial resolution of 0.8 mm. However, the correlation coefficient is lower at a spatial resolution of 0.1 mm. To resolve this question the image resolution of electrography and beta-radiography was further studied. The image resolution of electrographs and ^{14}C beta-radiographs was compared by their two-dimensional Fourier power spectrum. The normalized high frequency pass filtered two-dimentional Fourier power spectra of the electrograph and the ^{14}C beta-radiograph of sample #1 are shown in Fig. 18 together with their original images. The spectrum intensity of the electrograph was higher than that of the ^{14}C beta-radiograph in the high frequency region. This indicates that the image resolution of electrographs is higher than the ^{14}C beta-radiographs. This can be explained by the difference in direction of electron emission between the two methods. In the TEM the electron beam is made perpendicular to sample by an electro-magnetic lens system. On the other hand, since the ^{14}C beta-source is a wide plastic plate, the direction of electron emission is random, and this causes some blur in the beta-radiographs. Electrographs have an advantage over ^{14}C beta-radaiographs in image resolution.

Using statistics indicating formation, the electrographs and the beta-radiographs were compared at 0.4 mm spatial resolution and the results are shown in Table 5. The statistical parameters used are those of Cresson (32) and Gorres (14). It was found that the statistical values at both 0.4 and 0.8 mm spatial resolution are in good agreement with the printability data. It was also found that the electrographs and the beta-radiographs gave almost the same statistical values at these spatial resolution. However, a slightly larger difference in their values was observed at the higher spatial resolution (0.1 mm and 0.2 mm). This is caused by the difference in the image resolution of electrographs and beta-radiographs as mentioned above. Since the image resolution of the electrograph is higher than that of the beta-radiograph, the statistical values for the electrograph shows a higher variation.

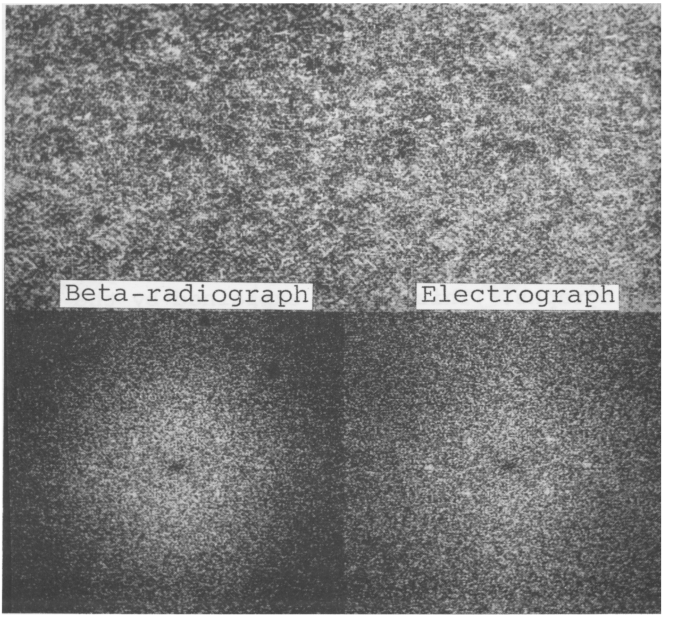

Fig.18 Comparison of two-dimentional Fourier power spectrum of the electrograph and the beta-radiograph for sample #1.

	Electrograph				Beta-radiograph			
Sample	#1	#2	#3	#4	#1	#2	#3	#4
First order statistics								
Coefficient of variation	0.12	0.13	0.13	0.14	0.11	0.12	0.12	0.12
Floc morphology								
Floc probability	0.23	0.26	0.32	0.28	0.25	0.24	0.33	0.34
Light weight zone probability	0.32	0.34	0.30	0.37	0.28	0.31	0.29	0.31
Edge probability	0.45	0.40	0.38	0.35	0.47	0.45	0.38	0.35
Floc size index (mm)	0.40	0.50	0.69	0.71	0.42	0.48	0.69	0.78
Floc distance index(mm)	1.75	1.96	2.12	2.23	1.71	1.89	2.10	2.30
Second order statistics								
Energy*100	0.35	0.30	0.24	0.19	0.37	0.32	0.29	0.27
Entropy	2.61	2.68	2.76	2.84	2.59	2.62	2.68	2.72
Correlation	0.35	0.48	0.54	0.56	0.34	0.47	0.55	0.61
Homogeneity	0.20	0.19	0.19	0.17	0.20	0.20	0.20	0.20
Contrast	36.4	34.4	38.6	45.1	32.5	32.9	30.7	32.2

Table 5 Statistics indicating formation of newsprint samples at 0.4 mm spatial resolution.

Some applications

Electrography was used to image the distribution of mass density of a paper sample of basis weight 205 g/m^2. The sample was heavily pressed and had some transparent spots. The object was to determine if the transparent spot is a high or a low basis weight zone. Since a ^{14}C beta-source cannot be used to image paper over 150 g/m^2, electron beams of 150 keV was used. A negative image of a light transmission and an electrograph of the sample are shown in Fig. 19. It was found that the transparent spots correspond to the high basis weight zone. Heavy pressing may have caused the transparent spots by eliminating the interfaces between fibers which contributes to opacity.

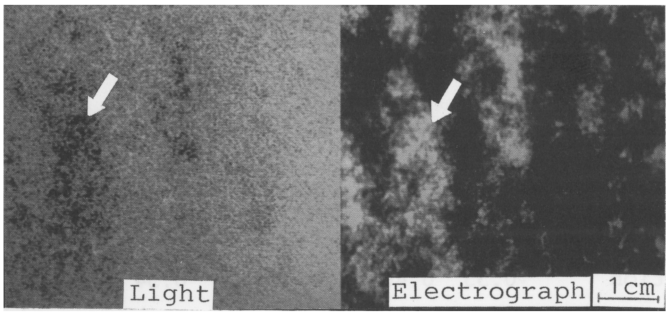

Fig.19 Light transmission image (negative) and electrograpn of the paper sample of basis weight 205 g/m^2.

TV Monitor system

Real-time imaging of the distribution of mass density by electron beams was performed with a TEM and a TV monitor system. The TV monitor system used here was developed for TEM real time imaging application, and has a sensitive area of 11 mm X 9 mm. A Mylar film wedge was carefully placed on the detector head and irradiated by electron beams with energies of 60 to 120 keV. The electron transmission image captured by the TV monitor system was sent to a image processing board and

digitized. The gray level of the image at each electron energy was normalized and plotted against the basis weight of the Mylar film as shown in Fig. 20.

It was found that a measurable basis weight range can be varied by changing the energy of electrons. This agrees with the result obtained for the photographic film system. However, in contrast to the case of photographic film system, no peak was observed in the basis weight calibration curve when the TV monitor system was used as a detector. The TV monitor system is equipped with a YAG screen to transform electrons into visible light. Since the YAG screen is thicker than the emulsion layer of photographic films and its average atomic number is higher than that of the emulsion layer, the YAG screen absorbs and detects electrons more efficiently than photographic films. The difference in the shape between these basis weight calibration curves is a result of the difference in the detector response. It is therefore very important to study the detector response to fully understand the performance of the system.

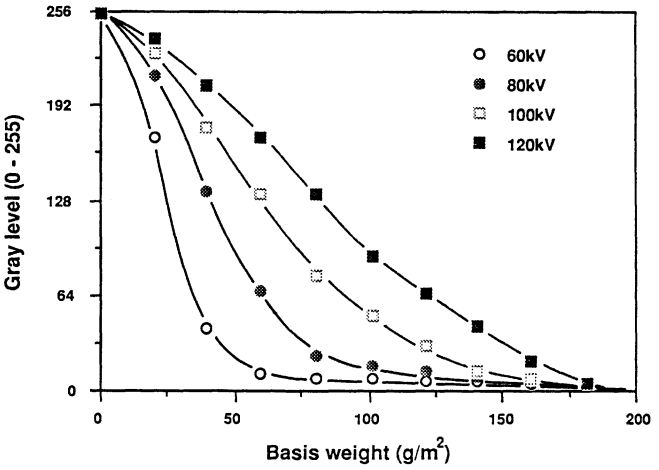

Fig.20 Basis weight calibration curve of Mylar film for various electron energies with the TV monitor system.

The newsprint sample #1 which is the same sample used for the comparison between the electrograph and the beta-radiograph was placed on the detector head and irradiated by electron beams with the energies between 60 keV and 120 keV. The images captured by the TV system are shown in Fig. 21. The actual sample size was 11 mm X 9 mm. Resolution of the images was sufficient and individual fibers could be recognized. However as mentioned above, the sample size measured is so small that statistical analysis of formation with these images is inappropriate and was not performed. If statistical information is required, development of a larger size fluorescent screen is necessary to image a larger sample.

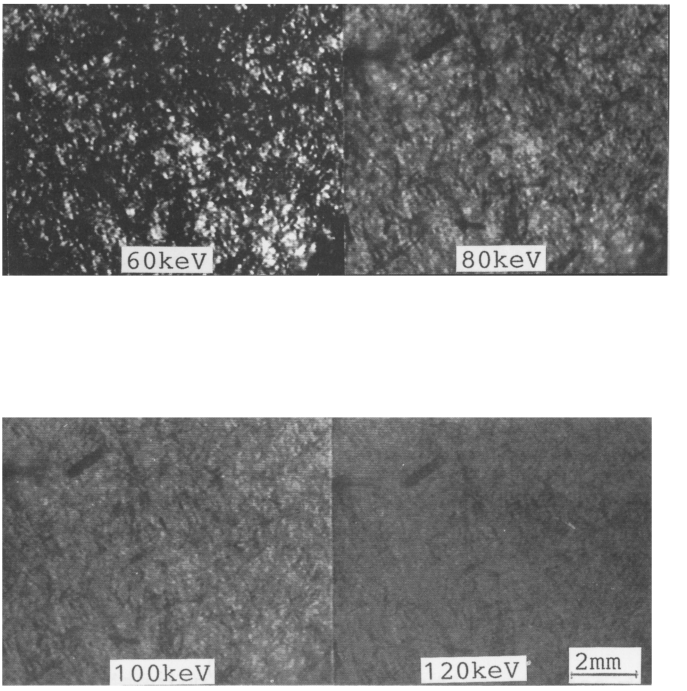

Fig.21 Real-time electron transmission image of sample #1 for various electron energies.

As shown in Fig. 21, contrast of the images decreased as the electron energy increased. On the other hand, it is indicated by Fig. 20 that the measurable basis weight range is higher for the higher electron energies. Therefore, if a detector system and image processing board have a high gray level resolution, i.e. 4096 gray levels (12 bit), a wide basis weight range can be acculately measured with one high energy electron beam.

CONCLUSION

Electron beams with energies ranging from 50 keV to 200 keV were found to be a suitable source to obtain the distribution of mass density of paper. The electron beam system has the following advantages over the beta-radiography system:

1. Exposure time can be reduced to 1 second or less (1/10,000 of exposure time for beta-radiograph).
2. Operation is very safe.
3. Wide range of basis weight can be covered (from 0 to 400 g/m^2).
4. Image resolution is higher than that of beta-radiograph.
5. Flux intensity distribution is very uniform over a wide area (variation is less than 5 %).
6. Real-time imaging of the distribution of mass density can be accomplished with a TV monitor system.

We can conclude that this technique has overcome many of the limitations of existing imaging methods to obtain the distribution of mass density of paper. Further development is required for a real-time imaging of larger paper samples.

ACKNOWLEDGEMENTS

The authors would like to thank Mitsubishi Paper Mills, Ltd. for supporting this work. The authors also thank Mr. Arnold C. Day at State University of New York, College of Environmental Science and Forestry, Ultrastructure Studies Laboratory for skillful TEM operation. We also gratefully acknowledge the support of Mr. Susumu Baba and Mr. Kunio Suzuki at Mitsubishi Paper Mills, Ltd. for supplying special experimental materials. The authors also would like to thank Dr. Peter Bergner and Mr. Terry Donovan at Gatan, Inc. for the use of the TV monitor system.

REFERENCES

1. Corte, H., Handbook of Paper Science, H. F. Rance ed., Elsevier, Amsterdam, (1980).

2. Norman, B. and Wahren, D., Tech. Sect. B.P.B.M.A., ed. Bolam, F., London, 7 (1973).

3. Sara, H., Ph.D. Thesis, University of Helsinki, March (1978).

4. Komppa, A. and Ebeling, K., Tech. Sect. B.P.B.M.A., ed. Bolam, F., London, (1981).

5. Herdman, P. T. and Corte, H., J. of Pulp and Paper Science, 81 (10), 81 (1980).

6. Herdman, P. T., Wiggins Teape Research and Development Ltd. Report, 1973.

7. Balodis, V., Appita, 18 (5), 184 (1965).

8. Aaltnen, P. and Simola, J., J. of Paper and Timber (Finland), 53 (9), 479 (1971).

9. Attwood, D. and Parker, J. R., Paper Technology, 3 (5), 435 (1962).

10. Tydeman, P. A., BP&BIRA Technical Bulletin, October (1964).

11. Yang, C. and Thorpe, J., Tappi J., 60 (12), 141 (1977).

12. Murata, M. and Nakata, K., 1981 Papermaking Conference (Japan Tappi and CPPA), Tokyo, October (1981).

13. Bergh, P. A., M.Sc. Thesis, State University of New York, College of Environmental Science and Forestry, Syracuse, (1981).

14. Gorres, J., Ph.D. Thesis, University of Manchester, (1983).

15. Marton, L. and Schiff, L. I., J. Applied Physics, 12 (10), 759 (1941).

16. Zeitler, E. and Bahr, G. F., J. Applied Physics, 30 (6), 940 (1959).

17. Zeitler, E. and Bahr, G. F., J. Applied Physics, 33 (3), 847 (1962).

18. Zeitler, E. and Bahr, G. F., Laboratory Investigation, 14 (6), 946 (1965).

19. Bahr, G. F. and Zeitler, E., Laboratory Investigation, 14 (6), 955 (1965).

20. Bahr, G. F., Engler, W. F., and Mazzone, H. M., Quarterly Reviews of Biophysics, 9 (4), 459 (1976).

21. Edie, J. W. and Karlsson, U. L., J. Microscopie, 13, 13 (1972).

22. Edie, J. W. and Karlsson, U. L., J. Microscopy, 11 (2), 179 (1977).

23. Linders, P. W. J., Zahniser, D. J., Stols, A. L. H., and Stadhouders, A. M., J. Histochemistry and Cytochemistry, 30 (7), 637 (1982).

24. Linders, P. W. J., Stols, A. L. H., and Stadhouders, A. M., J. Microscopy, 130 (1), 85 (1983).

25. Lapp, R. E. and Andrews, H. L., Nuclear Radiation Physics, Prentice-Hall, New Jersey, 139 (1963).

26. Boersch, H., Z. Physik, 139, 115 (1954).

27. Septier, A., Electron Microscopy in Material Science, Academic Press, New York, 15 (1971).

28. Birkhoff, R. D., Encyclopedia of Physics, Springer-Verlag, Berlin, 53 (1958).

29. Rohrlich, F. and Carlson, B. C., Physical Review, 93 (1), 38 (1954).

30. Berger, M. J. and Seltzer, S. M., NAS-NRC Publication, 1133 (10), (1964).

31. Zajac, B. and Ross, M. A. S., Nature, 164 (4164), 311 (1949).

32. Cresson, T. M., Ph.D. Thesis, State University of New York, College of Environmental Science and Forestry, Syracuse, (1988).

33. Bishop, H. E., British J. of Applied physics, 18, 703 (1967).

RAPID IMAGING OF MASS DISTRIBUTION IN PAPER BY ELECTRON BEAMS

H. Tomimasu, P. Luner and R. B. Hanna

Dr. D. Page, PPRIC

I would like to congratulate you on an excellent piece of work. It was done very thoroughly.
I have some previous experience in this area and am particularly interested in your efforts to simulate what happens when you use an electron beam to replace a carbon 14 source. I would like to put in a bit of history here on where the carbon 14 source came from. In 1960 I was an electron microscopist, and I took contact electron micrographs by taping the paper to the photographic plate as you did. We produced many images and they were very beautiful. However, there was only one electron microscope in the whole pulp and paper industry in England and therefore it was clear that it was not going to be a generally useful method. I then proceeded to search for a beta source to provide us with the same energy of beta rays. The Radiochemical Centre at Amersham (Now Amersham International) provided a carbon 14 dosed sheet of methacrylate and subsequently Peter Tydeman published work using this technique. This comment is not meant to detract from what you have done but it is amusing to me that we seem to have gone full circle. Perhaps the time is now right to use real time systems and using electron beams could prove to be a valuable tool.

A. Komppa, Finnish Pulp & Paper Research Institute

I congratulate you on your excellent research. I have a comment on the optical formation. You present in Table 3 some NUI figures for the samples as well as some figures for the printability. I imagine it was good to discover (from Table 5 of your results) your numbers for the morphology and second order studies for

formation nicely correlate with the printability, whereas the NUI figures do not. As Professor Norman pointed out, there is no way to measure formation using optical devices so hopefully with your new development we may have a tool which gives a true measure of mass formation.

Dr. M.B. Lyne, International Paper, USA

Having a monochromatic beam and being able to change the beam energy suggests spectroscopy. By changing the beam energy is it possible to differentiate between cellulose and clay or other filler materials, and could you conceive of your system being used to look at the formation of base stock in a coated paper or being able to look at filler distribution in uncoated papers independent of the cellulose?

H. Tomimasu

It is very difficult to use electron beams to differentiate various materials because the mass absorption coefficient of cellulose is very similar to filler. We can measure total mass but cannot differentiate the material. If you wish to differentiate materials I would suggest using soft X-rays rather than electron beams.

M.A. MacGregor, KTH (Voith)

I also congratulate you on a nice piece of work. With respect to your last answer does that mean that we cannot look at filled paper with this technique?

H. Tomimasu

There was a technique developed by Dr. Norman - he dissolved filler and measured the mass distribution before and after. I think this is the only technique we can use to measure filler distribution with electron beams.

M.A. MacGregor

If there is a masking effect of the filler on the cellulose we may not be getting a true representation of the cellulose distribution. However, I don't know of any other technique that can do that either.

Dr. A.H. Nissan, Westvaco, USA

I wondered if your electron beam could produce secondary X-rays which would distinguish between cellulose and fillers?

H. Tomimasu

The transition probability is very low - say 1/10,000 of the incident electron beam intensity so there is quite small chance of secondary X-rays.

Prof. D. Wahren, Stora Technology, Sweden

Did you not show us the mass distribution of a coating?

H. Tomimasu

Yes.

Prof. D. Wahren

It is not in the proceedings - can you tell us more about it?

H. Tomimasu

In fact this is a new project, can we discuss this afterwards?

P.T. Herdman, Wiggins Teape, England

Regarding filler distribution, there is a technique which is readily available to look at the distribution of fillers in paper. That is using a beta ray scanning device and replacing the beta ray source by a soft x-ray source. Iron-55 sources are available from Amersham International and the soft x-rays generated by them have appropriate energies for probing paper fillers. Interesting observations have been reported at the Harrison Hot Springs. TAPPI Physics Conference in 1979.

J.F. Waterhouse, Institute of Paper Science & Technology, USA

I would like to add my congratulations on a very nice piece of work. I would like to know whether you have actually considered electron beam curing equipment as a possible electron source for measuring formation on a continuous real time basis?

H. Tomimasu

For on-line measurement I think an electron flood gun for electron beam curing will be the best source since the intensity of the electron is very high. We do not have to worry about the absorption of electron energy by air.